

III-1

Accelerators and
Instruments

BL1U

Improvement of Image Quality of Selective Isotope 3D-CT in UVSOR-BL1U

H. Ohgaki¹, K. Ali¹, H. Zen¹, T. Kii¹, T. Hayakawa², T. Shizuma², M. Fujimoto³, Y. Taira³
and M. Katoh^{3,4}

¹*Institute of Advanced Energy, Kyoto University, Kyoto 611-0011, Japan*

²*Tokai Quantum Beam Science Center, National Institutes for Quantum and Radiological Science and Technology, Ibaraki 319-1106, Japan*

³*UVSOR Synchrotron Facility, Institute for Molecular Science, Okazaki 444-8585, Japan*

⁴*Hiroshima University, Higashi-Hiroshima 739-8511, Japan*

Nuclear Resonance Fluorescence (NRF) is a powerful tool to identify the specific isotope, especially in combination with a Laser Compton Backscattering (LCS) gamma-ray beam which provides quasi-monochromatic and energy variable gamma-rays. We have been developed an NRF-CT technique by using the LCS gamma-ray beam available at the beamline BL1U in UVSOR and demonstrated a three-dimensional (3D) isotope-selective CT image of the enriched lead isotope distribution of ²⁰⁸Pb in a cylindrical holder (Fig. 1), so far [1]. However, we needed 48 h beam time to obtain a CT image with a 4 mm/pixel in the horizontal plane and 8 mm/pixel in the vertical plane using the LCS gamma-ray beam with a beam size of 2 mm and a flux density of 10 photons/s/eV.

To overcome this problem, we proposed a fusion visualization (FV) technique by combining the NRF-CT image which provides a rough distribution of targeting isotope with a gamma-ray CT image which can be obtained by the same measurement system with NRF-CT but can provide better pixel resolution with a short measurement time (5 hours) [2]. We measured a 3D gamma-CT image of the same CT target [1] with the 3D NRF-CT in BL1U. The obtained 3D gamma-CT image (Fig. 2) has a 1 mm/pixel resolution with an LCS gamma-ray beam size of 1 mm and a flux density of 0.7 photons/s/eV. The target consists of two enriched lead isotopes (^{206,208}Pb), iron, and aluminum. As shown in Fig. 2, two enriched lead isotopes can be obtained but we cannot identify which one is the target isotope ²⁰⁸Pb.

After a few FV methods were applied to construct an FV image between NRF-CT and gamma-ray CT images, the post-multiply FV method which can keep the quantitative information of NRF interaction was selected. Figure 3 shows the 3D isotope-selective fused CT image. Consequently, we can improve the image quality of 3D NRF-CT of ²⁰⁸Pb rods embedded in the aluminum cylinder with ²⁰⁶Pb rod as well as iron rods with keeping quantitative information of NRF interaction.

[1] K. Ali *et al.*, “Three-Dimensional Nondestructive Isotope-Selective Tomographic Imaging of ²⁰⁸Pb Distribution via Nuclear Resonance Fluorescence.” *Appl. Sci.* **11** (2021) 3415. <https://doi.org/10.3390/app11083415>.

[2] K. Ali, *et al.*, “Fusion Visualization TecFighnique to Improve a Three-Dimensional Isotope-Selective CT Image Based on Nuclear Resonance Fluorescence with a Gamma-CT Image”, *Appl. Sci.* **11** (2021) 11866. <https://doi.org/10.3390/app112411866>.

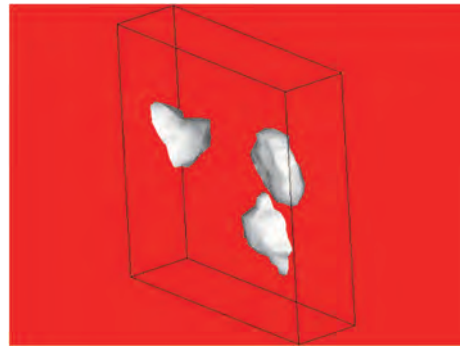


Fig. 1. 3D NRF-CT image measured in BL1U.

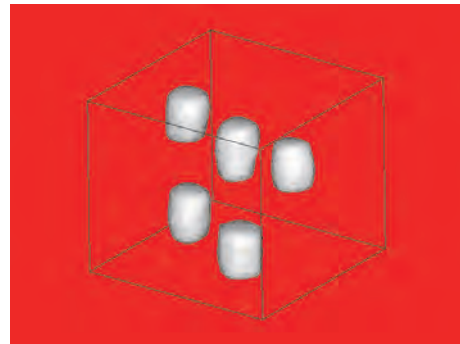


Fig. 2. 3D Gamma-ray CT image measured in BL1U.

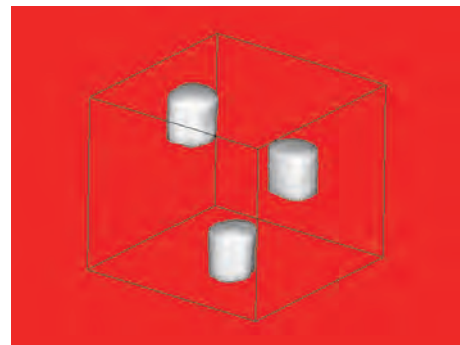


Fig. 3. 3D FV NRF-CT image

BL1U

Photon Counting Experiments of Young's Double-Slit Interference Using Undulator Vortex Radiation

S. Wada^{1,2}, H. Ohta², A. Mano³, M. Fujimoto^{4,3} and M. Katoh^{5,2,4}¹Graduate School of Advanced Science and Engineering, Hiroshima University, Higashi-Hiroshima 739-8526, Japan²Faculty of Science, Hiroshima University, Higashi-Hiroshima 739-8526, Japan³Synchrotron Radiation Research Center, Nagoya University, Nagoya 464-8603, Japan⁴UVSOR Synchrotron Facility, Institute for Molecular Science, Okazaki 444-8585, Japan⁵Hiroshima Synchrotron Radiation Center, Hiroshima University, Higashi-Hiroshima 739-0046, Japan

Recent theoretical and experimental progresses in the synchrotron radiation technology reveal that high harmonics emitted from a helical undulator possesses helical wave-front structure [1,2]. The undulator beamline BL1U at UVSOR can produce fundamental and its harmonics of circularly polarized radiation in visible and UV regions. Therefore, leading experiments using vortex radiation from the undulator have been conducted [3,4]. Especially, Young's double-slit interference experiments demonstrated the characteristic nature of vortex radiation as a singularity in the middle of the interference pattern arising from helical wave-front structure. This phenomenon is quite interesting from the view point whether a single photon spontaneously emitted from a high-energy electron can also possess such a characteristic or not. In this study, we demonstrated Young's double-slit experiments under photon-counting condition in order to confirm the above nature of vortex radiation from a helical undulator [5].

Experiments were performed at UVSOR BL1U under quite low-current mode (less than 1 mA). Circularly polarized radiation centered at 355 nm of second harmonics was extracted from a vacuum beamline to atmosphere via a quartz window, passed through an iris and an interference filter (Alluxa 7057) in order to extract center part and remove fundamental 710 nm light from the undulator radiation, and then irradiated onto a double-slit (0.1 mm width and 1 mm separation). By using as few optics as possible mentioned above, we could achieve very low simultaneous detection of two photons, that is single-photon counting condition in keeping helical wave-front structure. Single photons after interference were detected by a gated ICCD camera system (Hamamatsu Photonics, M7971-01 and ORCA-05G) 1 m far from the double-slits.

After confirming the double-slit interference in this experimental setup under multiphoton detection mode using a normal CCD camera, we could measure interference pattern even by photon counting detection as shown in Fig. 1(a). The figure was obtained by integrating 5000 shots of images with an exposure time of 200 μ s, and about 150 photons were randomly detected in each image. As clearly shown in the figure, we can find stripes due to interference by the double-slit and the singularity, that is mismatch of stripes at the dark middle region. The result obviously demonstrates that the interference patterns of circularly polarized

radiation from a helical undulator exhibit characteristics of optical vortex even under single-photon counting condition. The nature of vortex radiation from the undulator in the photon-counting condition is also confirmed by removing the double-slit as shown in Fig. 1(b), indicating the integrated beam profile like donut-shaped with the center missing. This is characteristic of vortex radiation with no light intensity due to a phase singularity.

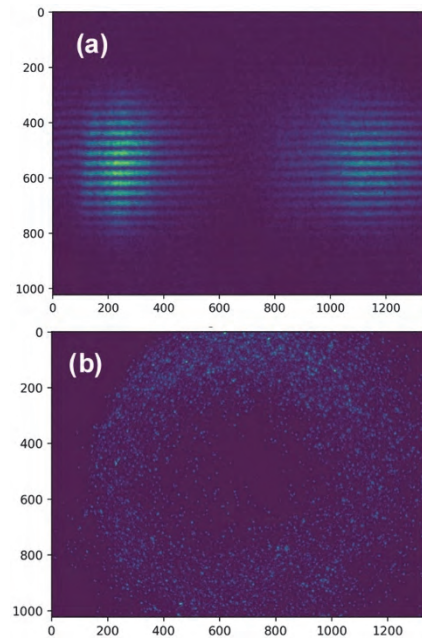


Fig. 1. (a) Young's double-slit interference pattern of vortex radiation measured at BL1U under photon-counting condition. (b) Integrated beam profile without the double-slit.

[1] S. Sasaki and I. McNulty, *Phys. Rev. Lett.* **100** (2008) 124801.

[2] J. Bahrtdt *et al.*, *Phys. Rev. Lett.* **111** (2013) 034801.

[3] M. Katoh *et al.*, *Sci. Rep.* **7** (2017) 6130.

[4] T. Kaneyasu *et al.*, *J. Synchrotron Rad.* **24** (2017) 934.

[5] H. Ohta, B.Sc. Thesis, Hiroshima University (2021).

Others

Development Mass Production Facilities of Nuclear Emulsion Films

I. Usuda, H. Rokujo and M. Nakamura

Graduate School of Science, Nagoya University, Nagoya 464-8602, Japan

Nuclear emulsion is a kind of photographic films that have sensitivity for ionizing radiation. The films record tracks of charged particle with high angular resolution.

In Nagoya University, we have developed gel production machine and developed several types of emulsion by ourselves. We are planning some experiments (e.g., gamma ray telescope, neutrino interaction research, muon radiography) using more than 500 m² nuclear emulsion films.

Nuclear emulsion is made by coating emulsion gel on plastic base. Previously, it was difficult to make large amount of films because we have coated emulsion gel by hand.

We have developed roll-to-roll coating machine in Nagoya University (Fig. 1). For mechanical coating, we have tried to add new chemicals to nuclear emulsion gel and optimize the gel's viscosity. We were the first in the world to succeed in the mechanical coating of over 60 μm thickness of nuclear emulsion films. We also introduced new gel production machine that can make 30 times amount of nuclear emulsion gel compared with conventional machine.

Now, we can make about 100 m² nuclear emulsion films per month.

We checked the performance of new emulsion gel and films. The index of sensitivity is Grain Density (GD) which is number of silver grains in the tracks of minimum ionized particle. The index of noise rate is Fog Density (FD) which is number of randomly generated silver grains unrelated to tracks. After we exposed electron beam to emulsion films at UVSOR (Fig. 2), we evaluated GD and FD.

We checked that GD and FD of nuclear emulsion gel and films which made by mass production facilities are comparable to that of conventional products. And the performance is stable for repeated operation. (Fig. 3, 4)



Fig. 1. Overview of roll-to-roll coating machine in Nagoya University.



Fig. 2. Optical microscopic image of electron beam (several tens of MeV) track. The electron beam was exposed at UVSOR.

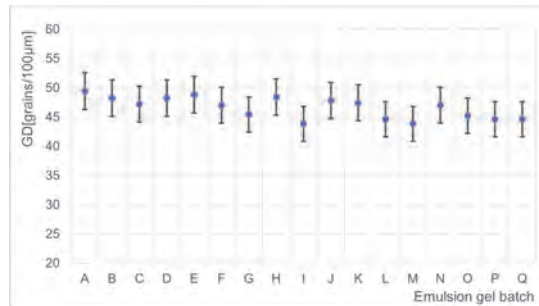


Fig. 3. Difference of Grain Density (GD) by emulsion gel batch.

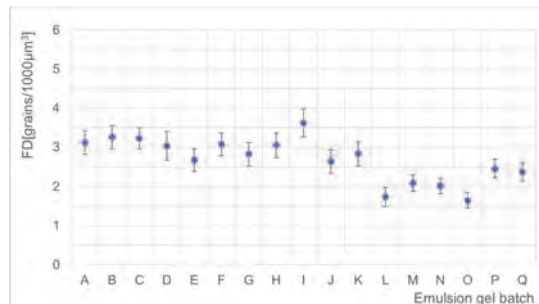


Fig. 4. Difference of Fog Density (FD) by emulsion gel batch.

III -1

BL1U

Laser Pulse Shaping and Transport at UVSOR-III

Y. Takashima^{1,2}, A. Mano¹, G. Jang², Y. Taira³, M. Fujimoto³, Y. Okano³ and M. Katoh^{4,3}

¹Synchrotron Radiation Research Center, Nagoya University, Nagoya 464-8603, Japan

²School of Engineering, Nagoya University, Nagoya 464-8603, Japan

³UVSOR Synchrotron Facility, Institute for Molecular Science, Okazaki 444-8585, Japan

⁴HiSOR, Hiroshima University, Higashi-Hiroshima 739-0046, Japan

We constructed the compact optics to shape a laser pulse to develop advanced Laser-Compton scattering gamma-ray source or sophisticated laser-synchrotron radiation combination experiment. The optics is a kind of Michelson interferometer [1]. As the first step, we tried to generate two temporally consecutive laser pulses (double pulse) from one original laser pulse. We confirmed generating double pulses.

Figure 1 shows the optics for the generation of the double pulse of the short-pulse laser. The original laser pulse is injected from the direction of arrow 1 in Fig. 1. The laser pulse is divided into the orthogonal direction "A" and "B" by the beam splitter in Figure 1; the laser pulses are reflected by the mirror 1 and 2. Mirror 2 is mounted on the movable stage so that the path length of the laser pulse along to "B" can be changed. The reflected pulses are mixed in the beam splitter and go through the direction "C", and then reflected the mirror 3 and exit to the direction "D".

We used an autocorrelator to measure the pulse width and the interval of the double pulses. The autocorrelator is installed downstream of the direction "D". According to the measurement using the autocorrelator, when we interrupt the laser pulse reflected on mirror 1, the FWHM of the pulse width of the laser of the single pulse is about 5.0 ps. Figure 2 showed the output signal from the autocorrelator when

we arranged the difference of the path length appropriately by moving the stage of mirror 2. We obtained the interval of the double pulse of about 3.0 ps. Fig. 3. shows the spectrum of the double pulse laser.

We successfully transported the laser pulse onto the circulating electron beam in the UVSOR-III storage ring by using the existing laser transport line for the Laser-Compton scattering.

III -1

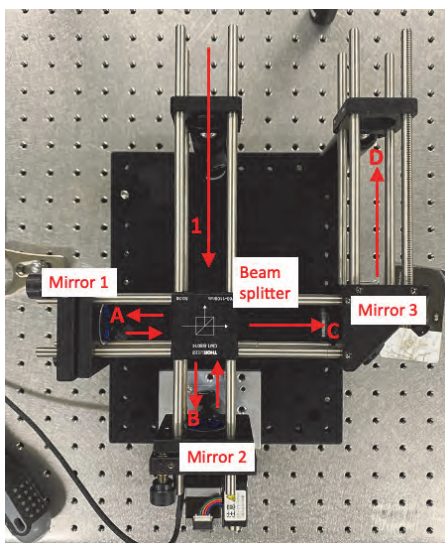


Fig. 1. Optics for the generation of the double pulse.

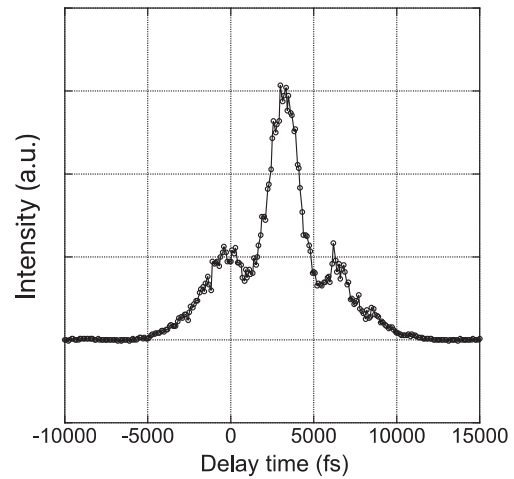


Fig. 2. The output signal of the autocorrelator.

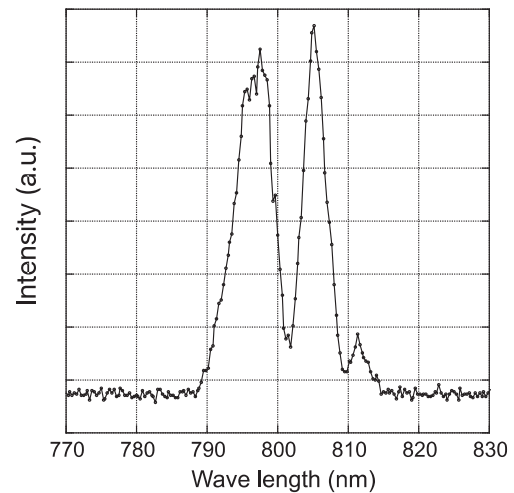


Fig. 3. The spectrum of the double pulse laser.

[1] G. Jang, Graduation thesis of School of Engineering, Nagoya University (2021)

BL1U

Revival of UVSOR-FEL and Gamma Ray Generation by Intra-cavity Laser Compton Scattering

H. Zen¹, J. Yamazaki², M. Fujimoto^{2,3}, K. Hayashi², H. Ohta², Y. Taira^{2,3} and M. Katoh^{2,4}

¹*Institute of Advanced Energy, Kyoto University, Uji 611-0011, Japan*

²*UVSOR Synchrotron Facility, Institute for Molecular Science, Okazaki 444-8585, Japan*

³*The Graduate University for Advanced Studies (SOKENDAI), Okazaki 444-8585, Japan*

⁴*Hiroshima Synchrotron Radiation Center, Hiroshima University, Higashi-Hiroshima 739-0046, Japan*

The lasing of Free Electron Laser (FEL) at S5 section was firstly achieved in 1992. The research activity related to FEL had been continued until the end of FY2011. Then the straight section used for activities of FEL and coherent light source developments was changed to S1, which has been newly created by moving the injection point. Two APPLE-II type undulators with an electromagnetic buncher magnet have been installed in the S1 section. The optical cavity used for FEL lasing was removed from S5 section at the end of FY2010 and reconstructed at the beginning of FY2015. In FY2017, we tried to have a first lasing of FEL at S1 section. At that time, we could achieve storage of undulator radiation in the optical cavity [1] but could not achieve FEL lasing due to a mismatch between the optical cavity length and the electron bunch interval. In the April-2021 shutdown of UVSOR, the position of the downstream mirror chamber was shifted to make the roundtrip frequency of the optical cavity the same as the electron bunch interval. In February 2022, a commissioning experiment of optical cavity and FEL was conducted to confirm the FEL lasing at S1 section.

The commissioning experiment of FEL was performed with an FEL cavity mirror pair which has high reflectivity around 520 nm. At first, the gap and the phase of the APPLE-II undulators are adjusted to have the center wavelength of 520 nm with the electron beam energy of 600 MeV. Next, the angles of the optical cavity mirrors were adjusted to store the undulator radiation in the optical cavity. Then the length of the optical cavity was scanned for finding the matching condition between the roundtrip frequency of the optical cavity and the electron bunch interval. This adjustment was performed with two bunch equidistant filling mode. The pulse duration of the stored light is strongly depending on the cavity length. The cavity length condition giving the shortest pulse duration of the stored light should be corresponding with the matched condition. After finding the matched condition of the cavity length, the electron beam current was increased up to 20 mA/2 bunch and the excitation current of the buncher magnet was increased up to 20 A. With a slight adjustment of the angle of the optical cavity mirror, lasing of the FEL can be achieved. Figure 1 shows the photograph of the FEL beam and its wavelength spectrum. The bright green spot in the photograph was the FEL beam having a central wavelength of 524.5 nm.

One of the interesting applications of UVSOR-FEL is the gamma-ray generation by the intra-cavity laser

Compton scattering [2]. In this study, two small current electron bunches were injected into 3 buckets behind the main bunches for generating gamma-ray by colliding with intra-cavity FEL beams. The spectrum of the generated gamma-ray measured by a NaI scintillator is shown in Fig. 2. The maximum gamma-ray energy was evaluated as 13 MeV. In this measurement, the optical cavity length was slightly detuned to avoid the pile-up events in the scintillator.

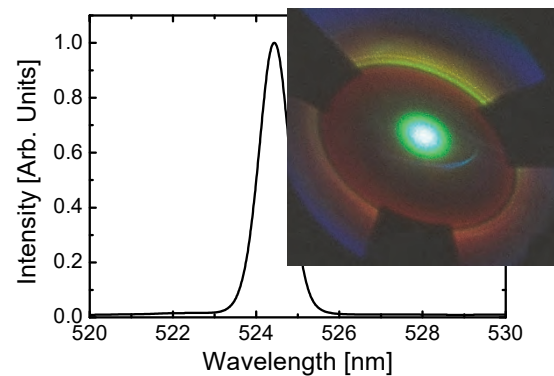


Fig. 1. Wavelength Spectrum and beam profile of FEL observed at the downstream of the optical cavity.

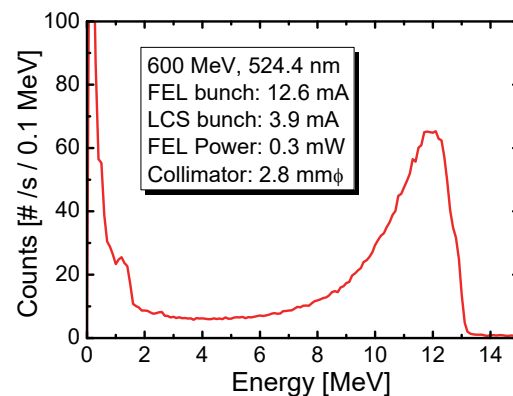


Fig. 2. The spectrum of the generated gamma-ray measured by a NaI scintillator.

[1] H. Zen *et al.*, UVSOR Activity Report 2017 **45** (2018) 31.

[2] M. Hosaka *et al.*, Nucl. Instrum. Meth. A **393** (1997) 525.

BL1U

Evaluation of Analyzing Power of Gamma-ray Polarimeter

S. Endo^{1,2}, T. Shizuma³, H. Zen⁴, Y. Taira⁵, K. Sugita⁵, O. Mohamed¹, S. Kawamura²,
R. Abe², T. Okudaira², M. Kitaguchi² and H. M. Shimizu²

¹Japan Atomic Energy Agency, Tokai 319-1195, Japan

²Nagoya University, Nagoya 464-8062, Japan

³National Institute for Quantum Science and Technology, Tokai 319-1195, Japan

⁴Kyoto University, Uji 611-0011, Japan

⁵Institute for Molecular Science, Okazaki 444-8585, Japan

A measurement of a circular polarization ratio of the gamma-rays emitted from an un-polarized neutron capture reaction of nuclei leads to the study for the compound nuclei [1]. Furthermore, the total angular momentum of neutron resonances can be determined by measuring the circular polarization ratio of gamma-rays from a polarized-neutron capture reaction [2]. We are aiming to conduct these measurements at J-PARC/MLF. The degree of the circular polarization of gamma-rays can be determined by measuring the transmission ratio of the magnet, called a gamma-ray polarimeter, because the cross-section of the Compton scattering depends on the direction of the electron polarization in the magnetized material and the gamma-ray helicity, i.e., circular polarization [3]. We developed a gamma-ray polarimeter and evaluated its analyzing power using a circularly polarized gamma-ray beam generated by the inverse Thomson scattering in the UVSOR BL1U [4].

The analyzing power is defined as

$$P_a = \frac{N^r - N^l}{N^r + N^l},$$

where N^r and N^l are the transmission ratio of the polarimeter for right- and left-circularly polarized gamma-rays, respectively. Figure 1 shows the schematic of the experiment. The beam flux was monitored by detecting gamma-rays scattered from brass with a LaBr detector. Gamma-rays transmitting the polarimeter were detected using a Ge detector. Figure 2 shows the gamma-ray energy spectrum taken by the Ge detector. Background measurement was performed with the laser off. Therefore, it includes the environmental radiation and backgrounds derived from the Bremsstrahlung. The pile-up effect was corrected, and the transmission ratio was obtained from the number of events for the LaBr and Ge detectors.

Since the analyzing power depends on the magnetic field, it depends on the current flowing the polarimeter. Figure 3 shows the obtained analyzing power for each current for 100% circularly polarized gamma-rays. The current up and down mean whether the current was increased or decreased, respectively, reflecting the effect of magnetic hysteresis. The analyzing power was obtained as $P_a = 2.12 \pm 0.04\%$ above 2 A.

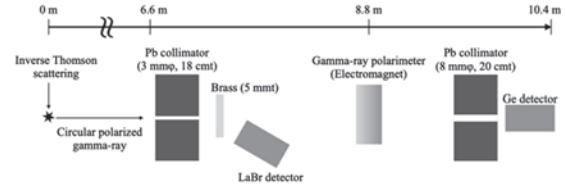


Fig. 1. Schematic of experimental setup.

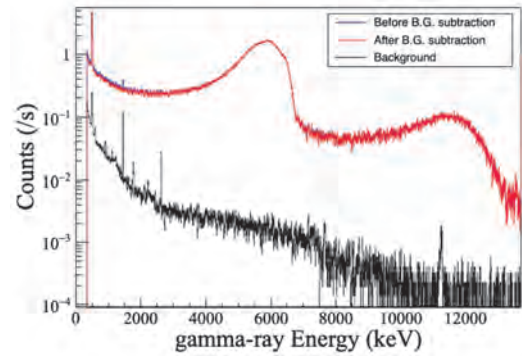


Fig. 2. Gamma-ray energy spectrum taken by the Ge detector.

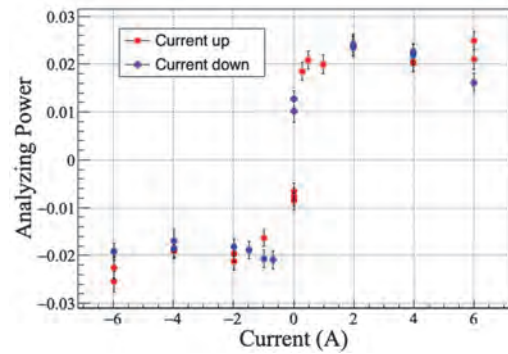


Fig. 3. Analyzing power for each current.

[1] V.V. Flambaum and O.P. Sushkov, Nucl. Phys. A **435** (1985) 352.

[2] L.C. Bindenham *et al.*, Phys. Rev. **83** (1951) 683.

[3] H.A. Tolhoek, Rev. Mod. Phys. **28** (1956) 277.

[4] Y. Taira *et al.*, Nucl. Instrum. Meth. Phys. Res. A **637** (2011) 116.

BL1U

Development of Gamma ray Induced Positron Annihilation Spectroscopy

Y. Taira^{1,2}, K. Sugita^{1,2}, R. Yamamoto³, Y. Okano¹ and T. Hirade⁴

¹UVSOR Synchrotron Facility, Institute for Molecular Science, Okazaki 444-8585, Japan

²School of Physical Sciences, The Graduate University for Advanced Studies (SOKENDAI), Okazaki 444-8585, Japan

³Graduate School of Engineering, Nagoya University, Nagoya, 464-8603, Japan

⁴Nuclear Science and Engineering Center, Japan Atomic Energy Agency, Tokai, 316-8511, Japan

Positron annihilation spectroscopy (PAS) is an excellent method to detect lattice defects in solids such as vacancies, dislocations, and clusters and free volumes in polymers [1]. Conventional β^+ radioisotopes such as ^{22}Na , a positron beam generated from an electron accelerator, and a high energy gamma ray [2,3] are used for PAS. PAS using a high energy gamma ray, which is called gamma ray induced PAS (GiPAS), has several advantages compared with PAS using conventional radioisotopes. (i) It enables defect analysis of a thick material in a few centimeters because positrons are created throughout a bulk material via pair production by irradiation with gamma rays having high penetration into the material. (ii) Source contribution of positrons annihilated in the covering material is negligible. In conventional radioisotopes, about 10 % ~ 15 % of positrons annihilate in the source. This distorts the positron lifetime spectra and complicates the data analysis.

Inverse Thomson/Compton scattering is a scattering process between high energy electrons and a laser, which can produce high energy gamma rays. A MeV gamma ray can be generated by the scattering between a 1 GeV electron and a 1 eV photon. The generated gamma rays possess features such as quasi-monochromatic and tunable energy, highly polarized, low divergence angle, and low background. Inverse Thomson/Compton scattered gamma rays have been generated at several electron accelerator facilities in the world. We have developed ultra-short pulsed gamma rays by inverse Thomson scattering at UVSOR-III [4]. They are generated via inverse Thomson scattering with 90 degree collisions between a 750-MeV electron beam and a Ti:Sa laser pulse. The maximum energy is 6.6 MeV and the pulse width is calculated to be sub-ps to ps ranges.

We are currently developing GiPAS using the ultra-short pulsed gamma ray [5]. Gamma ray induced positron annihilation lifetime spectroscopy (GiPALS), which is a technique to measure positron lifetime and evaluate type of defects at the nanometer scale and their concentrations inside material, is currently available for users. The measured positron lifetime spectrum of stainless steel distributed by National Metrology Institute of Japan (NMIJ) as reference material for positron lifetime is shown in Fig. 1. The positron lifetime spectrum was analyzed using LT9 program.

In addition to GiPALS, we have developed gamma

ray induced age-momentum correlation (GiAMOC), which is a technique to measure time resolved momentum distribution of an electron which is the annihilation counterpart of a positron. The measured AMOC spectrum of the NMIJ stainless steel is shown in Fig. 2.

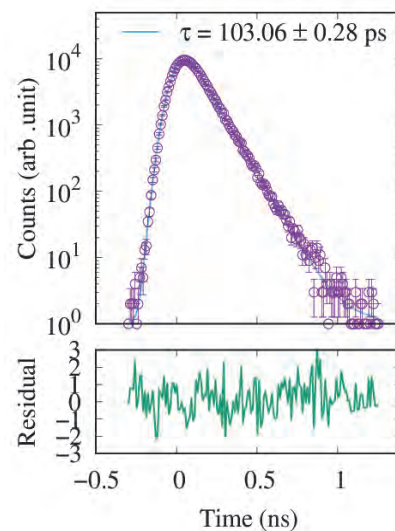


Fig. 1. Measured positron lifetime spectrum of NMIJ stainless steel. Time resolution is 138 ps in full width at half maximum.

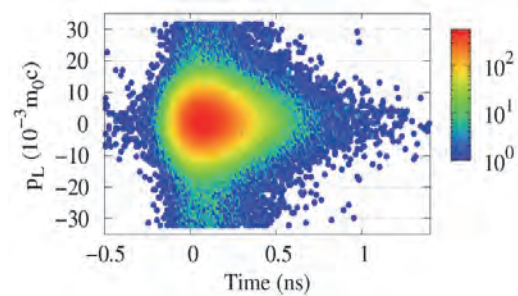


Fig. 2. GiAMOC spectrum of NMIJ stainless steel.

- [1] J. Cizek, *J. Mat. Sci. Tech.* **34** (2018) 577.
- [2] F. A. Selim, *Acta Phys. Pol. A* **132** (2017) 1450.
- [3] M. Butterling *et al.*, *Nucl. Instr. Meth. Phys. Res. B*, **269** (2011) 2623.
- [4] Y. Taira *et al.*, *Nucl. Instr. Meth. A* **652** (2011) 696.
- [5] Y. Taira *et al.*, *Rev. Sci. Instr.* **84** (2013) 053305.

BL1U

Single Electron Storage at UVSOR-III

R. Shinomiya¹, M. Shimada^{2,3}, H. Miyauchi^{2,3}, M. Fujimoto⁴ and M. Katoh^{3,1,4,2}

¹*School of Science, Hiroshima University, Higashi-hiroshima 739-8526, Japan*

²*High Energy Accelerator Research Organization (KEK), Tsukuba 305-0801, Japan*

³*Hiroshima Synchrotron Radiation Research Center, Hiroshima University, Higashi-hiroshima 739-0046, Japan*

⁴*UVSOR Synchrotron Facility, Institute for Molecular Science, Okazaki 444-8585, Japan*

Single electron storage in an electron synchrotron (electron storage ring) has been achieved at several facilities, aiming to investigate electron dynamics in a synchrotron [1,2], to investigate electromagnetic radiation from an electron [3,4], or to utilize the radiation as a primary standard [5,6]. However, in Japan, as far as we know, there is no report on such studies.

We have tried the single electron storage at UVSOR-III aiming to establish accelerator techniques for this special operation mode toward novel experiments in future.

The experimental procedure is as follows. First, we accumulate an electron beam with relatively low current, typically around 1 mA. Then, we reduce the beam current by using a device called beam scraper, which is a movable copper rod installed on the beam pipe at a straight section. We can insert the rod into the beam pipe close to the beam from the vertical direction. When we make the distance between the rod and the beam around 1 mm, the beam lifetime becomes several minutes, which is much shorter than the normal one, typically several hours. We observe the beam current by using DCCT until around 0.1 mA. Below this beam current, the DCCT cannot give reliable data. Then, we use a photomultiplier tube (PMT) to measure the synchrotron radiation intensity at BL1U, where ultraviolet radiation can be produced from an undulator. The wavelength of the fundamental radiation from the undulator was set to be 355 nm. The PMT was set at a small dark room surrounded by black curtains, where the undulator radiation was extracted from the ultra-high vacuum chamber of the beamline to the air through a sapphire window. The signal from the PMT was analyzed with a counting unit and was recorded by a PC. We tried to apply various bandpass filters to improve the signal to noise ratio. We found that a bandpass filter which had a moderately large bandwidth of about 60 nm and passed almost all the fundamental component of the undulator radiation gave the best result.

We mounted four ND filters with OD 2.0 on the PMT at the start of the measurement. As decreasing the beam current, we removed them one by one as keeping the counting rate of PMT lower than the limit of the processing rate of the counting unit. After removing all the ND filters, we successfully observed step-function-like jumps in the time history of the counting rate as shown in Fig. 1, which indicated the loss of the electrons one by one. The background rate is much smaller than the step of the counting rate, which corresponds to the

radiation intensity emitted from one electron. The observed counting rate from one electron was consistent with a preliminary evaluation of the photon flux based on an analytic formula.

We do not describe the details here, but we also succeeded in observing which RF bucket the last electron existed in. Moreover, after confirming that only one electron is circulating, we pulled out the beam scraper and observed that the last electron was stored for more than 2 hours, which is sufficiently long to carry out the experiments with single electron.

In conclusion, we successfully demonstrated the single electron operation at UVSOR-III and establish the basic techniques for this special operating mode. We are going to start novel researches utilizing this new mode.

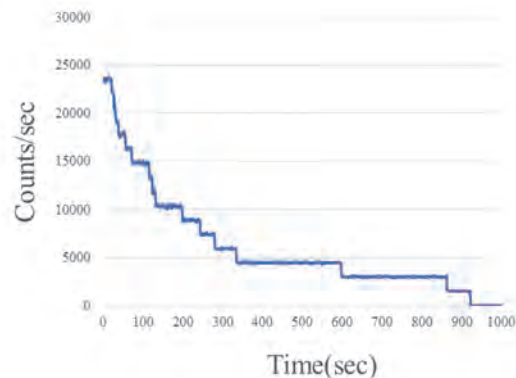


Fig. 1. Synchrotron radiation intensity at BL1U.

- [1] A. N. Aleshaev *et al.*, NIM A **359** (1995) 80.
- [2] I. V. Pinayev *et al.*, NIM A **375** (1996) 71.
- [3] I. V. Pinayev *et al.*, NIM A **341** (1994) 17.
- [4] A. Romanov *et al.*, JINST **16** (2021) P12009.
- [5] R. Klein *et al.*, Phys. Rev. STAB **11** (2008) 110701.
- [6] R. Klein *et al.*, Metrologia **47** (2010) R33.

BL1U

Exploring Novel Application of Undulator Radiation Based on Interferometric Technique

K. Kato¹, M. Shimada^{2,3}, H. Miyauchi^{2,3}, A. Mano⁴ and M. Katoh^{3,1,5,2,4}

¹*School of Science, Hiroshima University, Higashi-hiroshima 739-8526, Japan*

²*High Energy Accelerator Research Organization (KEK), Tsukuba 305-0801, Japan*

³*Hiroshima Synchrotron Radiation Research Center, Hiroshima University, Higashi-hiroshima 739-0046, Japan*

⁴*Synchrotron Radiation Research Center, Nagoya University, Nagoya 464-8603, Japan*

⁵*UVSOR Synchrotron Facility, Institute for Molecular Science, Okazaki 444-8585, Japan*

The classical electromagnetic theory indicates that radiation from a relativistic electron running in an undulator forms a wave packet whose number of cycles is exactly same as the number of magnetic periods of the undulator. In case of the undulator at BL1U, the number of the magnetic period is 10. If we set the wavelength of the fundamental radiation at 355 nm, then the wave packet has a length of 3.5 micron which corresponds to about 10 femtosecond. This “ultrafast” property of synchrotron radiation has merely been considered useful for any applications except for only a few previous works [1]. However, recently, at UVSOR, interesting applications of this property has been demonstrated successfully [2,3,4].

Following these successes, we continue exploring other possible applications. We were inspired by a previous study using interferometer, in which the undulator radiation showed a clear interferogram [5]. We started considering an application to the tomographic imaging. In the optics technology field, a technology called optical coherence tomography has been successfully demonstrated and are widely used particularly in the medical field [6]. Its principle may be described as follows. A low coherence light beam splits into two by means of a beam splitter. Two beams are reflected by mirrors and come back to the beam splitter and merge. When the path lengths are exactly same, interference fringe is observed in the merged beam. If a sample material is inserted on a path, because of the refractive index of the sample, the path length which gives the interference changes. Moreover, if multi-reflection takes place in the sample, interference is observed at several different path lengths. From such observation, one can get information on the inner structure and its optical property of the sample. We have carried out a proof of principle experiment on such a tomography method using undulator radiation at BL1U [7]. Some preliminary results are presented here.

The wavelength of the undulator radiation was selected at 355 nm, which is compatible with the wavelength range of the Mach–Zehnder interferometer, which was constructed in a previous study [5]. We utilized the existing interferometer to observe the change of the interferogram as putting samples on its light paths. We tried two configurations, transmitting and reflecting ones. To minimize the modification of the interferometer, in the former configuration, we just

placed the sample on the one of the path after the beam splitter, and, in the latter, we placed the sample at the reflecting mirror.

We carried out the interferogram measurements on some thin materials such as glass plates or films and several stimulated samples which has multilayer structure. One example of the interference fringe is shown in Fig. 1. In this measurement, a thin film is placed in a transmitting configuration. The sample covered a half of the light path. By adjusting the optical path length, we could observe interference fringe only for the half area where the film existed. More details will be presented in future papers.

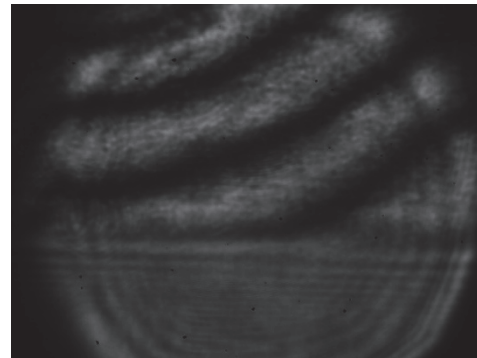


Fig. 1. Interference fringe observed for 25 micron OPP film as a sample. In the upper side, the OPP film is placed and in the lower none.

- [1] S. Nakanishi *et al.*, *J. Synchrotron Rad.* **5** (1998) 1702.
- [2] T. Kaneyasu *et al.*, *Phys. Rev. Lett.* **123** (2019) 233401.
- [3] Y. Hikosaka *et al.*, *Nature Comm.* **10** (2019) 4988.
- [4] T. Kaneyasu *et al.*, *Phys. Rev. Lett.* **126** (2021) 113202.
- [5] *e.g.* D. Huang *et al.*, *Science* **254** (1991) 1178
- [6] A. Mano *et al.* *UVSOR Activity Report 2020* **48** (2021) 38.
- [7] K. Kato *et al.*, presented at JSR 2022 (2022).

BL2A

Calibration of CMOS Sensor with Reflective-type Flux Reduction System

N. Narukage

National Astronomical Observatory of Japan, Mitaka 181-8588, Japan

The solar corona is full of dynamic phenomena such as solar flares. The understandings of these phenomena have been progressing step-by-step with the evolution of the observation technology in EUV and X-rays from the space. But there are fundamental questions remain unanswered or haven't even addressed so far. Our scientific objective is to understand underlying physics of the dynamic phenomena in the solar corona, covering some of the long-standing questions in solar physics such as particle acceleration in flares and coronal heating. To achieve this objective, we identify the imaging spectroscopy (the observations with spatial, temporal and energy resolutions) in the soft X-ray range (from ~ 0.5 keV to ~ 10 keV) is a powerful approach for the detection and analysis of energetic events [1]. This energy range contains many lines emitted from below 1 MK to beyond 10 MK plasmas plus continuum component that reflects the electron temperature.

The soft X-ray imaging spectroscopy is realized with the following method. We take images with a short enough exposure to detect only single X-ray photon in an isolated pixel area with a fine pixel Silicon sensor. So, we can measure the energy of the X-ray photons one by one with spatial and temporal resolutions. When we use a high-speed soft X-ray camera that can perform the continuous exposure with a rate of more than several hundred times per second, we can count the photon energy with a rate of several 10 photons / pixel / second. This high-speed exposure is enough to track the time evolution of spectra generated by dynamic phenomena in the solar corona, whose lifetimes are about from several ten seconds to several minutes. For the first imaging spectroscopic observation of the solar corona in soft X-ray range, we launched a NASA's sounding rocket (FOXSI-3) on September 7th, 2018 and successfully obtained the unprecedented data [2] using a high-speed X-ray camera [3] with a back-illuminated CMOS sensor [4].

Calibration of CMOS detectors is essential for scientific data analysis. For this purpose, a completely monochromatic X-ray light source is needed. In addition, the flux must be adjusted so that individual X-ray photons can be isolated. Therefore, so far, we have controlled (reduced) the flux by adjusting the material and thickness of metal filters. However, in this case, the lower energy was preferentially attenuated, so the contamination of higher-order (2nd, 3rd and 4th order) components could not be removed, resulting in incomplete data for calibration.

In this time, we developed a mirror-based reflective-type flux reduction system (see Fig. 1). In this system, two flat mirrors aligned in parallel are mounted on a rotating stage, and by changing the angle of incidence, the reflectance, i.e., attenuation rate, can be flexibly

adjusted. The system worked well as expected and successfully produced the completely monochromatic light with the appropriate flux. As a result, the response of the CMOS detector used in the FOXSI-3 sounding rocket project could be completely calibrated in the energy range of 830 eV to 4500 eV in 50 eV intervals (see Fig. 2).

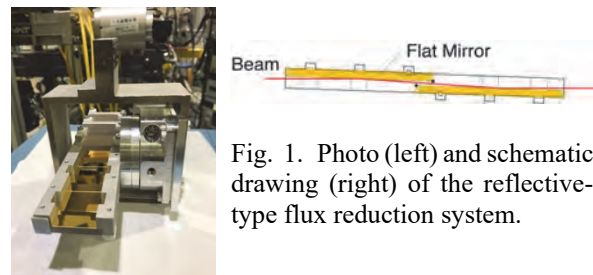


Fig. 1. Photo (left) and schematic drawing (right) of the reflective-type flux reduction system.

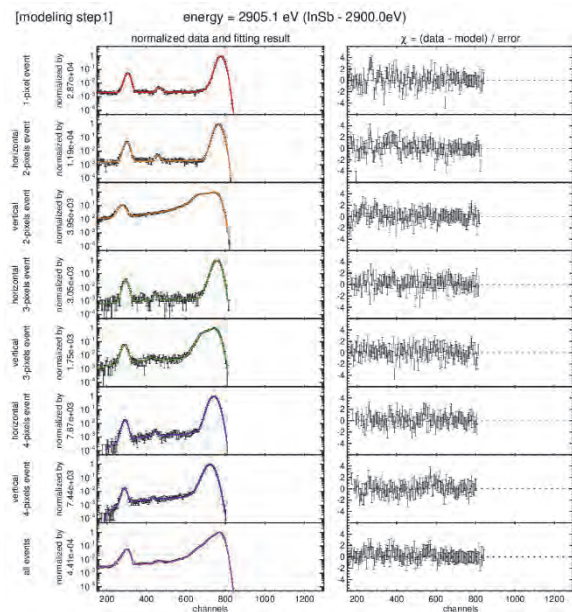


Fig. 2. Measured (black data points) and modeled (colored lines) response of the CMOS sensor to the monochromatic X-rays (at 2905.1 eV in this case).

[1] N. Narukage *et al.*, White paper of the “soft X-ray imaging spectroscopy”, arXiv:1706.04536 (2017).

[2] N. Narukage and S. Ishikawa, UVSOR Activity Report 2018 **46** (2019) 36.

[3] S. Ishikawa *et al.*, Nuclear Instruments and Methods in Physics Research Section A, **912** (2018) 191-194.

[4] N. Narukage *et al.*, Nuclear Instruments and Methods in Physics Research Section A, **950** (2020) 162974.

BL3B

Photon Energy Resolutions of BL3B Evaluated by Appearance Energy Measurements of Xe⁺ Ions

H. Iwayama^{1,2}¹UVSOR Synchrotron Facility, Institute for Molecular Science, Okazaki 444-8585, Japan²School of Physical Sciences, The Graduate University for Advanced Studies (SOKENDAI), Okazaki 444-8585, Japan

A beamline in a synchrotron facility generally works as a monochromator and focus system. A photon energy resolution of the beamline is one of the most important parameters for various measurements. To maintain the performance of the beamlines, it is desirable to check the actual photon energy resolution regularly.

The beamline BL3B can provide monochromatic light in the range from visible to extreme ultraviolet region. Previously the photon energy resolution of BL3B was evaluated by vibration-rotation spectra of oxygen molecules [1], which are significantly complex. In this work, we estimate photon energy resolutions of BL3B from appearance energy spectra, which have step functional structure at an ionization threshold.

The photoelectron-photoion coincidence (PEPICO) measurements for an ion time-of-flight mass spectrum were performed at UVSOR BL3B. A schematic view of PEPICO measurements is described in the previous report [2]. Sample gas is xenon, whose ionization threshold is 12.130 eV [3]. The ion mass spectra were recorded at photon energies ranging from 12.100 eV to 12.200 eV in 0.001 eV-increments. We used G1 grating of BL3B. We estimate photon energy resolutions for three slit configurations of (entrance slit, exit slit) = (500 μm , 500 μm), (300 μm , 300 μm) and (100 μm , 100 μm).

Figure 1 shows a typical mass spectrum of Xe ions. The peak structure results from an isotope distribution of Xe atoms. The corresponding mass resolution $m/\Delta m$ is 400.

Figure 2 shows Xe ions yield spectra for three slit configurations. We find steep rises at the ionization threshold of 12.130 eV. With narrowing slit sizes, steps of Xe ion yield spectra become steeper. This shows that photon energy resolution become better. From three spectra, we estimate photon energy resolutions for three slit configurations and summarize Table 1. In future, we also perform estimations of photon energy resolutions for G2 and G3 gratings.

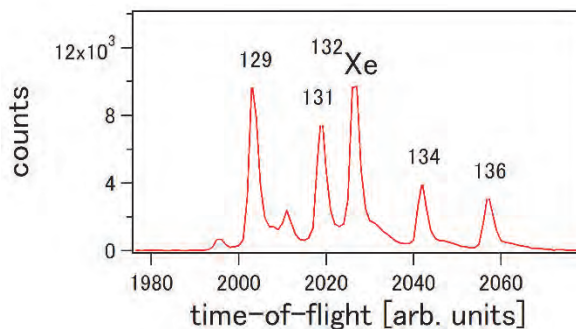


Fig. 1. Typical time-of-flight mass spectrum of Xe ions.

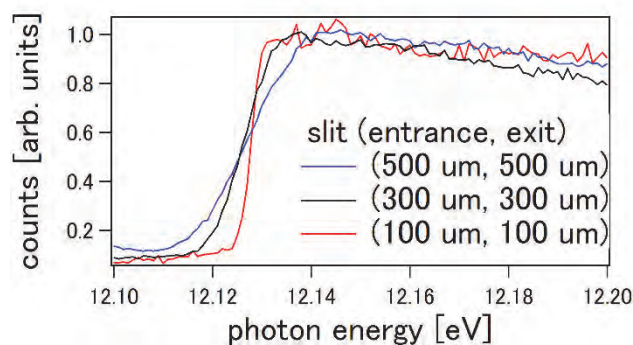


Fig. 2. Xe ion yield spectra around the ionization energy of 12.130 eV for three slit configurations.

Table 1. Photon energy resolutions for G1 grating

Slit size	ΔE @ $h\nu=12\text{eV}$	$E / \Delta E$
(500 μm , 500 μm)	20 meV	600
(300 μm , 300 μm)	11 meV	1000
(100 μm , 100 μm)	4.2 meV	3000

[1] K. Fukui, *et al.*, *J. Synchrotron Rad.* **21** (2014) 452.

[2] H. Iwayama and T. Horigome, *UVSOR Activity Report 2020* **48** (2021) 41.

[3] https://physics.nist.gov/PhysRefData/ASD/levels_form.html.

BL4B

BL4B Usage for Developing the Photoelectron Spectroscopy End-station for Organic Materials

K. Fukutani, H. Iwayama, F. Matsui and S. Kera
Institute for Molecular Science, Okazaki 444-8585, Japan

The field of organic electronics has been prolific in the last couple of years. However, the study of the molecular function and property using the synchrotron light sources has been limited so far due to difficulty in the measurements for irradiation sensitive materials and lack of the suitable environment for the comprehensive experiments.

The soft X-ray beamline BL4B, monochromator was designed to cover the energy range of 35 – 800 eV and used for XMCD and XAS by setting the user apparatus. To achieve the fundamental understanding of charge transport properties, adsorption properties, interface energetics, chemical reactivity and so on, we placed the end-station with the acceptance-cone-tunable electron spectrometer (ACTES) for the highly efficient constant-energy photoelectron mapping based on the ARPES system equipped with a hemispherical analyzer (MBS A-1 Lens4) [1].

In the initial process, we tested the figure of merit for a typical experimental procedure, that is core-level photoelectron spectroscopy, valence band energy-band dispersion measurement, low-energy secondary electron cut-off measurement with bias voltage, and near-edge X-ray absorption fine structure (NEXAFS) spectroscopy. The samples of Au(111) and molecular films of OV-phthalocyanine (OVPC) are prepared.

The photon flux is moderate at BL4B, however it is still high enough to make some troubles on the sample of organic films, like an irradiation damage. We have checked a typical measurement condition of photon flux and analyzer parameters with energy resolution and spectral intensity for optimizing the molecular systems. The beam-spot size was set at 0.68 x 0.52 mm at photon energy ($h\nu$) of 60 eV with a resolution power ($E/\Delta E$) of 5,000. Effective low- $h\nu$ range could start from 30 eV, and it would be very hard to obtain the results at 25 eV for ARPES experiments. The high- $h\nu$ range could be useful up to 1,200 eV for XPS experiments, though the monochromator covers up to 1,500 eV. The contribution of the second-order light is estimated less than 1 % for $h\nu = 250$ eV at the $E/\Delta E$ of 2,000 for grating G1.

XAS was demonstrated for C-, N-, and O- K edges. A large photon-flux dropping due to a mirror contamination is observed for C-K edge region, and the NEXAFS experiments for bulk samples could be reasonable by changing the irradiating position slightly for recording the data by using a relatively clean area of the gratings, however we request to clean up the mirror systems. Moreover, the reference data of Au mesh must be clarified to obtain the data for thin-film interfaces.

The beam stabilities of the photon energy and flux

have been carefully checked by repeatedly measuring the binding energy and intensity of Au 4f and Fermi edge. The result confirms that the light will be stabilized after about 1 hour. The continuous scanning for accumulating the data long time under the low-photon flux should be confirmed again.

The beam damage on the molecular film sample is checked for the annealed monolayer of OVPC/Au(111) with $h\nu = 60$ eV at the $E/\Delta E$ of 2,000, which gives the sample current (I_s) of 5.2 nA (corresponding to the Au mesh current (I_0) of 167 pA). We observed discernible broadening of the HOMO spectral feature over the 2 h irradiation as shown in Fig. 1. We find the irradiation effects are settled by reducing the photon flux to the $I_s = 0.55$ nA to give no remarkable change in the features over 40 min. The impact will depend on the $h\nu$ range, hence the molecular film survived for 60 min. in XPS for $h\nu = 500$ eV at the $E/\Delta E$ of 2,000, giving the $I_s = 0.28$ nA ($I_0 = 32$ pA), but not suitable for a higher-photon flux of $I_s = 0.77$ nA ($I_0 = 85$ pA) as an example.

The detailed experiments upon cooling the sample will be continued in FY2022.

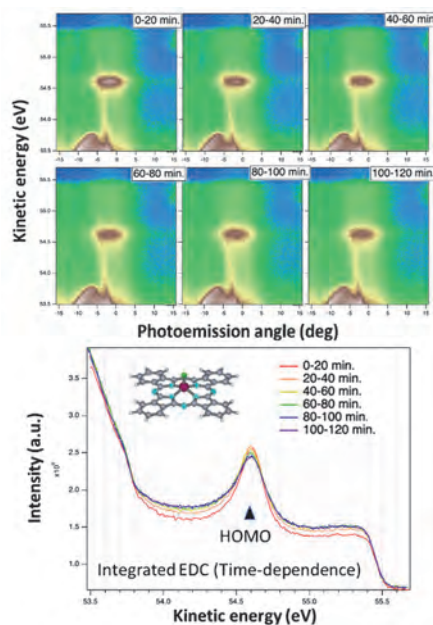


Fig. 1. Impacts of irradiation time on the ARPES of a monolayer of OVPC/Au(111) surface taken at 295 K and $h\nu = 60$ eV.

[1] H. Yamane *et al.*, *Rev. Sci. Instrum.* **90** (2019) 093102.

BL4B

Development of High Efficiency Liquid Cell in Total Electron Yield Using Atomically-thin Graphene

I. Mitsuishi¹, K. Kashiwakura¹, Y. Niwa¹, T. Ogawa¹, Y. Tawara¹, R. Kitaura², P. Solís-Fernández³, K. Kawahara³, H. Ago³, T. Taniguchi⁴, K. Nomoto⁴, H. Kodaka⁴, T. Horigome⁵, E. Nakamura⁵, H. Iwayama⁵, M. Nagasaka⁵ and K Tanaka⁵

¹ Graduate School of Science, Division of Particle and Astrophysical Science, Nagoya University, Nagoya 464-8602, Japan

² Department of Chemistry, Nagoya University, Nagoya 464-8602, Japan

³ Global Innovation Center, Kyushu University, Kasuga 816-8580, Japan

⁴ Optical Measurement Technology Development Department, R&D Division, USHIO INC., Yokohama 225-0004, Japan

⁵ UVSOR Synchrotron Facility, Institute for Molecular Science, Okazaki 444-8585, Japan

X-rays are a powerful probe to investigate material properties through, e.g., X-ray absorption spectroscopy (XAS) which can reveal local atomic and electronic states of oxygen, carbon, etc.. Among the XAS methods for liquid, total electron yield is preferably utilized in some cases because short electron escape depth in this method makes it possible to examine atomic and electron states of liquid surface and solid-liquid interfaces. In order to realize high efficiency measurements through the total electron yield method, high efficiency films with high electron transmission are a key and therefore have been strongly desired.

To construct our original device for the total electron yield measurements, we propose to utilize graphene which is atomically thin and has high electron transmission [1]. As a first step, we tried to establish our original experimental setup to verify our idea as shown in Fig. 1. As a preliminary experiment, liquid water was sandwiched by a silicon nitride window and free-standing 5-layer graphene on a quartz substrate with apertures of 0.5 x 0.5 mm. A high voltage system was also prepared between the entrance window of the sample and the X-ray source to reduce the contamination of electrons produced by the surface of the substrate and sample holder. We obtained the spectra around the O K-edge structure as shown in Fig. 2 and confirmed the O K-edge absorption by the liquid water. However, photoelectrons of oxygen were also detected in background spectra without the sample. Thus, to reduce the contamination, voltages of 200, 400, 600, and 800 eV were applied and the reduction of the commination was confirmed successfully as shown in Fig. 2. Although the high-voltage system worked well and the contamination level went down significantly, we could not conclude that there is no significant contribution to the observed photoelectrons with the sample. Thus, to evaluate the sensitivity of our liquid cell, optimizations of our experimental setup based on simulations are necessary.

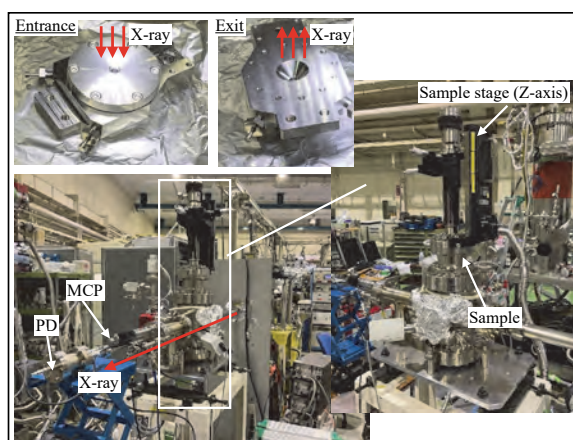


Fig. 1 Experimental setup and an overview of the sample holder.

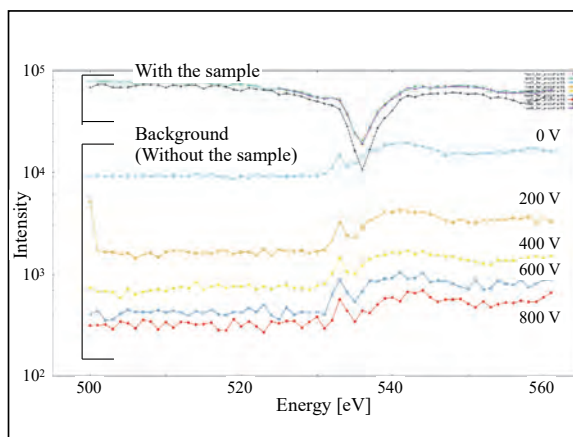


Fig. 2 Examples of observed MCP spectra around the O K-edge structure with / without the sample. The spectra with voltages of 200, 400, 600, 800 eV are also shown for comparison.

[1] G. Hassink, R. Wanke, I. Rastegar, W. Braun, C. Stephanos, P. Herlinger, J. H. Smet and J. Mannhart, *APL Materials* **3** (2015) 076106.

BL5B

Development of a Fluorescence Polarimeter in Extreme Ultraviolet Region

T. Kaneyasu¹, K. Hosaka² and J. Adachi³

¹SAGA Light Source, Tosu 841-0005, Japan

²National Institutes for Quantum Science and Technology, Takasaki 370-1292, Japan

³Institute of Materials Structure Science, KEK, Tsukuba 305-0801, Japan

Polarization is one of the most important characteristics of synchrotron radiation. In addition to the use of horizontal linear polarization in the bending magnet radiation, the recent advent of insertion devices allows us to use arbitrarily polarized light in a wide spectral range from vacuum ultraviolet to x-ray. For accurate measurements using the polarization properties of synchrotron radiation, it is essential to evaluate the polarization state of light at a sample point. Here, we present a polarization measurement of synchrotron radiation in the extreme ultraviolet (XUV) wavelength region using a fluorescence polarimeter. This method is based on the conversion of the XUV radiation to visible radiation on the atomic resonance [1-3]. The fluorescence preserves the polarization state of the excitation light when it is observed along the light propagation axis. Comparing with the optical polarimeters [3], this method has advantages in its simple apparatus and easy operation.

The experiment was performed at the bending magnet beamline BL5B in UVSOR synchrotron. Figure 1 shows the experimental layout of the present study. The monochromatized synchrotron radiation interacted with helium atoms provided by an effusive beam. The pressure of the interaction chamber was around 1×10^{-3} Pa during the measurement. The excitation wavelength was 51.56 nm, corresponding to the 1s5p resonance of helium atom. We observed 361-nm-wavelength fluorescence photons emitted in decays from 1s5p to 1s2s state of a helium atom. The fluorescence photons emitted parallel to the light propagation axis (z-axis) were detected by a photomultiplier tube equipped with a polarizer and a bandpass filter. To evaluate the polarization state of XUV radiation, we measured fluorescence intensity as a function of the rotation angle of the polarizer.

Figure 2 shows the fluorescence intensity measured as a function of the polarizer angle which is defined by the angle of the polarization axis with respect to the horizontal axis (x-axis). The fluorescence intensity shows a sinusoidal modulation reflecting the polarization state of the XUV radiation. Assuming an elliptical polarization, the experimental data points are fitted by a theoretical curve. The linear polarization degree of light is evaluated to be 0.74 which is somewhat smaller than the ideal value of 0.84 [4]. This disagreement is probably due to the detection solid angle for the fluorescence photons, and it is expected that this instrumental effect can be improved by reducing the detection solid angle.

The present work shows the capability of a fluorescence polarimeter to evaluate the polarization state of XUV radiation. Although we evaluated the degree of linear polarization only, this method has the potential to determine Stokes parameters [3] by just introducing a quarter waveplate in the detector system.

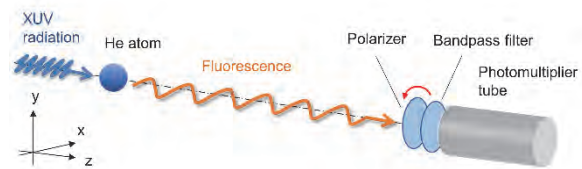


Fig. 1. Experimental layout of the present study. The fluorescence photon emitted along the light propagation axis was detected.

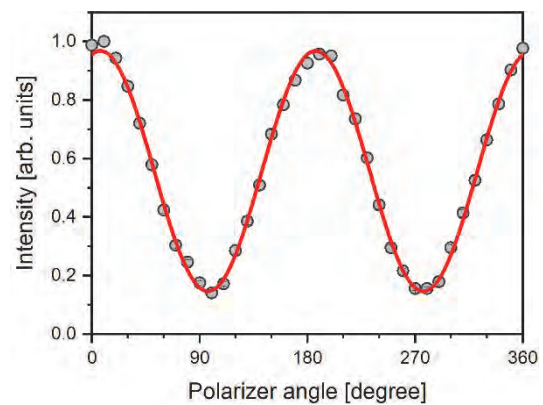


Fig. 2. Fluorescence intensity measured as a function of the polarizer angle. The experimental data points are fitted by a theoretical curve.

- [1] V. Bobahev and O. S. Vasyutinkii, *Rev. Sci. Instrum.* **63** (1992) 1509.
- [2] C. J. Latimer et al., *J. Electron Spectroscopy Relat. Phenom.* **101-103** (1999) 875.
- [3] E. Allaria et al., *Phys. Rev. X* **4** (2014) 041040.
- [4] Y. Hikosaka et al., *J. Synchrotron Rad.* **27** (2020) 675.

BL5B

Measurement of a Detection Efficiency of High-sensitivity Microchannel Plates with Tapered Pores

S. Matoba¹, H. Iwayama^{2,3} and T. Kaneyasu⁴

¹*Institute of Materials Structure Science, KEK, Tsukuba 305-0801, Japan*

²*Editorial Board, UVSOR Synchrotron Facility, Institute for Molecular Science, Okazaki 444-8585, Japan*

³*School of Physical Sciences, The Graduate University for Advanced Studies (SOKENDAI), Okazaki 444-8585, Japan*

⁴*SAGA Light Source, Tosu 841-0005, Japan*

A microchannel plate (MCP) is a lead glass detector with a two-dimensional array of electron-multiplying pores of about 10 μm in diameter. When charged particles or short-wavelength photons collide with the inner wall of the pore, secondary electrons are generated and amplified in the pore to be detected as electron pulses. MCPs are used in a very wide range of fields from basic research to industry because of their large area, high spatial resolution, and high-speed detection capability. The maximum detection efficiency of an MCP is at the upper limit of its open-area-ratio, and typical MCPs have a detection efficiency of 50-60%. This causes a problem of reduced detection efficiency when used in coincidence measurement experiments. For example, if an MCP with a detection efficiency of 60% is used in a triple coincidence experiment, the total detection efficiency drops to about 20%. We have developed a tapered MCP with an effective aperture of 89% by applying a tapered aperture to the incident area, based on the idea that the detection efficiency can be increased by increasing the aperture. The maximum detection efficiency of the tapered MCP for monatomic ions was improved to 90%, comparable to the open-area-ratio, demonstrating for the first time the effectiveness of tapered processing in the detection of monatomic ions [1]. MCPs are also used as UV and X-ray detectors, and are employed as imaging elements for planetary atmosphere observation from satellites and spacecraft. It is known that a CsI coating on the surface of an MCP improves the detection efficiency by several tens of times in the wavelength region above 100 nm, but below 100 nm, where emission lines from helium and oxygen ions, which are major components of many astronomical atmospheres, are concentrated, the improvement is only 1.2 times [2]. Therefore, it is not a decisive observation method for understanding the dynamic picture of celestial atmospheres. In this experiment, the detection efficiency of EUV is measured using a tapered MCP to verify its usefulness. The wavelength range of about 32-190 nm was used for the measurement. Spectrified EUV passes through a pinhole with a diameter of 1 mm and is injected into the MCP. Since the counting rate of the MCP saturates at high intensity, a molybdenum mesh and a Kapton thin film were used to attenuate the light. A 300-nm-thick aluminum foil was inserted to attenuate higher-order light. The MCP used for the measurement is a custom-made type divided into four regions: normal type,

tapered type, CsI-coated normal type, and CsI-coated tapered type.

Figure 1 shows the intensity ratios of the measured count rates of tapered MCP (T-MCP), CsI-coated MCP (CsI-MCP), and tapered CsI-coated MCP (TCsI-MCP) to normal-type MCP (N-MCP). The detection efficiency of the tapered MCP is higher than that of the normal MCP in all the measured wavelength ranges. In the short wavelength range, the tapered MCP has a higher detection efficiency than the CsI-coated MCP. The synergistic effect of tapered MCP and CsI coating on the detection efficiency of MCP was confirmed. These results demonstrate that tapered MCP is a powerful tool for UV detection.

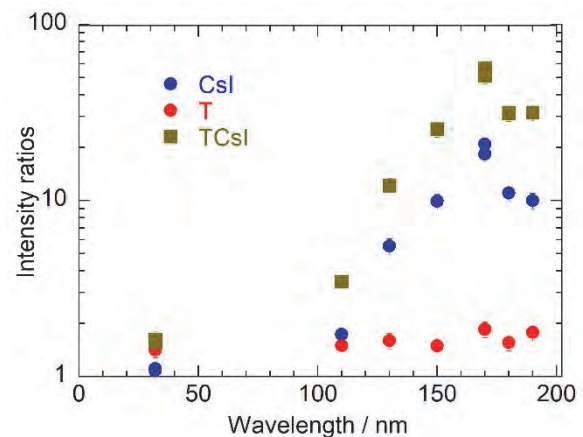


Fig. 1. intensity ratio of measured count rates of tapered MCP (T), CsI-coated MCP (CsI) and tapered CsI-coated MCP (TCsI) to normal type MCP (N-MCP).

[1] S. Matoba *et al.*, *Jpn. J. Appl. Phys.* **50** (2011) 112201.

[2] K. Yoshioka *et al.*, *Rev. Sci. Instrum.* **83** (2012) 083117.

BL5B

Study on the Source of Photon-Energy Drift of BL5B

H. Zen¹, E. Nakamura², K. Hayashi² and K. Tanaka^{2,3}

¹*Institute of Advanced Energy, Kyoto University, Uji 611-0011, Japan*

²*UVSOR Synchrotron Facility, Institute for Molecular Science, Okazaki 444-8585, Japan*

³*School of Physical Sciences, The Graduate University for Advanced Studies (SOKENDAI) Okazaki 444-8585, Japan*

The stability of the photon beam properties, such as beam position, beam intensity, photon energy, and so on, during user operation in beamlines, are very important for the advanced application of synchrotron radiation (SR) facilities. A photon-energy drift at BL5B has been observed during user experiments [1]. We started the study on the source of this photon-energy drift in 2019. Although we have tried several countermeasures to suppress the photon-energy drift [2], no significant improvement has been achieved.

In the study performed FY2020, we found a clear correlation between the temperature of the M1 mirror holder and the photon energy [3]. Therefore, in this FY, a heater attached directly to the M1 mirror holder was introduced to control the temperature of the M1 mirror holder. By using the heater, the temperature of the M1 mirror holder can be stabilized as shown in Fig. 1 (a) black line. However, even with the stabilized M1 temperature, the wavelength of the SR exit the monochromator continuously changes as shown in Fig. 1 (c) black line and red line.

To find the origin of the photon-energy drift, several trials were made; 1: Turn off and on the heater on M1 holder, 2: Remove M1 mask to increase the M1 holder temperature, 3: decrease mirror temperature by reducing SR amount on M1 and successive optics. By trial 1, we could confirm the correlation between M1 holder temperature and the photon energy. By trial 2, we found that the temperature variation of the M1 holder has no significant influence on the trend of photon-energy drift. By trial 3, we found that the variation of SR amount has a significant influence on the photon energy drift. After reducing the SR amount, the temperature of the M1 mirror gets stable within 3 hours (see Fig. 1 (b) red line) but the photon-energy drift last for longer than 6 hours (see Fig. 1 (c) red line). These results imply that the significant source of the photon-energy drift should exist after the M1 mirror.

We checked our results obtained in FY2019. In FY2019, grating #3 and mirror #23 (configuration of G3M3) were used and roughly 0.1 eV photon-energy drift was observed from 12 to 21 o'clock. In this FY, roughly 0.24 eV photon-energy drift was observed from 12 to 21 o'clock with grating #2 and mirror #24 (G2M4). The sensitivity of the photon energy to the angular variation for the G2M4 configuration is approximately 1.2 times higher than that of the G3M3 configuration. The observed difference of photon-energy variation was much larger than the difference of sensitivity. From this result, grating and its holding

mechanics are considered to be a significant source of the photon-energy drift of BL5B. Further study should be conducted to clarify whether the grating and its holding mechanics are the significant sources of the photon-energy drift or not.

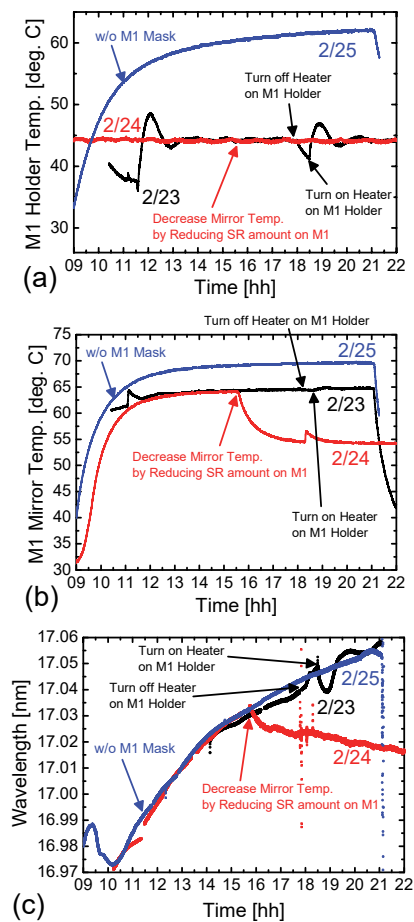


Fig. 1. Trend of (a) temperature of M1 mirror holder, (b) temperature of M1 mirror, and (c) wavelength of SR light exit monochromator of BL5B.

[1] K. Hayashi, UVSOR Activity Report 2011 **39** (2012) 121.

[2] H. Zen *et al.*, UVSOR Activity Report 2019 **47** (2020) 42.

[3] H. Zen *et al.*, UVSOR Activity Report 2020 **48** (2021) 47.

BL7B

Complex Refractive Index Measurement by Reflectance Spectra in Different Polarization Configurations

M. Horiba¹, K. Fukui¹, K. Yamamoto¹ and T. Saito²

¹Department of Electrical and Electronics Engineering, University of Fukui, Fukui 910-8507, Japan

²Department of Electrical and Electronic Engineering, Tohoku Institute of Technology, Sendai 982-8577, Japan

Based on the basic design of the instrument by the AIST group [1], we have been developing a complex type refractive index spectrum measurement device (CRIMS-VUV) [2], which can continuously measure not only in the visible region but also in the ultraviolet and vacuum ultraviolet regions. CRIMS-VUV can perform spectroscopic ellipsometry measurements and reflection spectrum measurements under the same environment.

The spectroscopic ellipsometry measurement mode of CRIS-VUV has the advantage of measuring the complex refractive index with high accuracy. However, this mode has the disadvantage that, due to its measurement principle, it takes time to measure at each measurement point (photon energy), making it difficult to measure a continuous spectrum. In this respect, reflection spectrum measurement mode is suitable for measuring continuous spectrum. The well-known Kramers - Kronig analysis method is used to determine the complex refractive index spectrum from the reflectance spectrum. However, Kramers - Kronig analysis method requires appropriate approximations on both sides of the measured photon energy range, since Kramers - Kronig analysis method uses the integral of reflectance at photon energy from 0 to infinity to obtain complex refractive index at each photon energy. Therefore, this method is useful, for example, for obtaining qualitative complex refractive index spectrum for limited photon energy region around the absorption edge, but is not well suited for obtaining quantitative complex refractive index spectrum over a wide photon energy region. Unlike the Kramers - Kronig analysis method, there are two methods to obtain the complex refractive index at each photon energy from reflectance measurements under different measurement conditions, one with reflectance measurements at different incident angles and the other with different polarization configurations. Therefore, we decided to use a method of measuring reflectance with *p*- and *s*-polarization configurations (PS method) to obtain the complex refractive index for each photon energy, since CRIMS-VUV has a mechanism that automatically changes the polarization configuration as desired. In this report, we show the trial results of PS method measurements on an Au mirror as a sample.

PS method measurements were carried out with CRIMS-VUV installed at BL7B. The photon energy range was 2 to 20 eV. Since output light of BL7B (input light of CRIMS-VUV) is highly linearly polarized

(Stokes parameter $S_1/S_0 \sim 0.8$), reflectance measured in the horizontal and the vertical configuration are almost equal to the reflectance of *p*- and *s*-polarization, respectively.

The reliability of complex refractive index derived from experimental values is directly related to the magnitude of the difference in reflectance in *p*- and *s*-polarization configuration. Therefore, the angle of incidence should be close to Brewster's angle, and experiments have confirmed that the difference in reflectance spectra between the *p*- and *s*-polarization configuration increases in the order of 8°, 45°, and 67° angle of incidence. Therefore, results for 45° and 67° are used for analysis. Figure 1 shows the photon energy dependence spectra of complex refractive index of Au mirror. The curves represent refractive index *n* and extinction coefficient *k* derived from PS method, and symbols from spectroscopic ellipsometry measurement mode. The overall trend of *n* and *k* spectra from PS method are in good agreement with those from spectroscopic ellipsometry measurement mode. However, a marked difference in absolute values remains an issue to be solved.

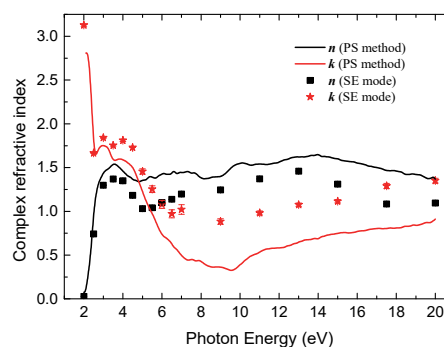


Fig. 1. Complex refractive index of Au mirror

[1] T. Saito, M. Yuri and H. Onuki, Rev. Sci. Instrum. **66** (1995) 1570.

[2] D. Imai *et al.*, UVSOR Activity Report 2018 **46** (2019) 39.

UVSOR User 3

